CrystEngComm

ROYAL SOCIETY OF CHEMISTRY

PAPER

View Article Online
View Journal | View Issue

Cite this: *CrystEngComm*, 2021, **23**, 5116

Cl^--Induced selective fabrication of 3D AgCl microcrystals by a one-pot synthesis method†

Jiye Wang,[a] Yazhou Qin, *[a] Qiaocui Shi,[a] Luhong Wen[bc] and Lei Bi[bc]

The controllable preparation of crystals is a prerequisite for exploring their shape-dependent physicochemical properties. Herein, AgCl crystals with different morphologies including octahedron, trapezohedron (TPH), 12-pod and hexapods with mace pods were successfully prepared by a one-pot synthesis method. In the preparation process, ethylene glycol (EG) was used as a solvent and $AgNO_3$ was used as a precursor of Ag^+. In particular, the ionic liquid poly(diallyldimethylammonium chloride) (PDDA) not only acted as a Cl^- ion precursor but also as a morphology-controlled stabilizer. We further explored the effects of temperature, ligand and precursor concentration on AgCl crystal growth. Moreover, we investigated the effect of Cl^- concentration on the morphology of AgCl by adding different amounts of NaCl. We found that under the condition of the lower concentrations of Cl^-, {111}-bound octahedral AgCl crystals will transform into TPH enclosed with the {311} facet as the concentration of Cl^- ions increases. However, at medium concentrations of Cl^-, {111}-bound octahedral AgCl crystals will transform into 3D 12-pod AgCl crystals as the concentration of Cl^- ions increases. Under the condition of higher concentrations of Cl^-, {111}-bound octahedral AgCl crystals will transform into hexapods with mace pods AgCl crystals as the concentration of Cl^- ions increases. According to the experimental results, we proposed the growth mechanism of AgCl microcrystals. This work not only provides a new method for the synthesis of AgCl crystals with a tunable shape, but also helps to understand the crystal growth mechanism.

Received 27th October 2020,
Accepted 24th June 2021

DOI: 10.1039/d0ce01564d

rsc.li/crystengcomm

Introduction

In the past few decades, the controllable preparation of micro/nanomaterials has become an important research field. In particular, a large number of studies have been devoted to the controllable preparation of micro/nanocrystals because of their potentially wide variety of applications including catalysis, photonics, sensing and imaging.[1–6] It is well established that the properties of crystals depend largely on their surface structure.[7–10] Previous studies have shown that crystals with a high index facet have higher chemical reaction activities than those with low index facets, as the high-index facet crystals have a much higher density of low-coordination stepped atoms, ledges and kinks.[11] However, the high surface energy of high-index planes makes them disappear easily in the growth process to minimize the total surface energy.[12] As a result, the synthesised crystals are usually enclosed by low-index facets such as {100} and {111} surfaces. Therefore, it is extremely difficult and challenging to synthesize crystals with specific high-index facets. More recently, with great efforts, many noble metal (Au, Ag, Pt and Pd) crystals with different morphologies of high-index facets including dodecahedra (DDH), tetrahexahedra (THH), trisoctahedra (TOH), hexoctahedra (HOH) and truncated ditetragonal prism (TDP) have been prepared by electrochemical and wet-chemical methods.[13–17] Among many micro/nanomaterials, silver chloride (AgCl), a promising semiconductor photocatalytic material, has been extensively studied due to its excellent photocatalytic properties. Since the solubility of AgCl is low (the solubility product constant at 25 °C is 1.77×10^{-10}),[18] it is usually prepared by a precipitation reaction between Ag^+ and Cl^- ions. However, because the precipitation reaction is already fast, the controllable preparation of AgCl is still a challenge. In 2008, Huang and co-workers first founded that Ag@AgCl particles are active plasmonic photocatalysts.[19] Since then, silver halides, in particular AgCl, have been considered as the most promising substitute for traditional semiconductor photocatalysts. Many studies have focused on the preparation of AgCl crystals with different morphologies to study their photocatalytic activity under visible light irradiation. Up to now, extensive research has shown that surface plasmon resonance (SPR) induced electron transfer and, thus, led to high photocatalytic activity of AgCl.[20–24] In

[a] *Key Laboratory of Drug Prevention and Control Technology of Zhejiang Province Zhejiang Police College, China. E-mail: yazhouqin@zju.edu.cn*
[b] *Ningbo University, China*
[c] *China Innovation Instrument Co., ltd., China*

† Electronic supplementary information (ESI) available. See DOI: 10.1039/d0ce01564d

addition, many kinds of well-defined AgCl micro/nanocrystals including nanospheres,[25] cubes,[26–28] plates,[29–31] caged cubes[32,33] and nanowires[34–36] have been synthesised and they showed significant photocatalytic activity in the degradation of organic pollutants under visible light irradiation. For example, Yu prepared heart-like Ag@AgCl crystals, which exhibit enhanced visible light photocatalytic performance.[37] Lou and co-workers prepared concave cube AgCl microcrystals by controlling the cubic seed to grow preferentially along the <111> and <110> directions under the action of highly concentrated Cl^- solution.[38,39] Moreover, Gatemala *et al.* prepared various kinds of highly branched three-dimensional AgCl hierarchical microcrystals.[40] Interestingly, the results indicate that three-dimensional AgCl hierarchical superstructures exhibit better catalytic performance than common cubes and octahedrons. Therefore, in order to explore and realize the potential applications of novel structural materials, there remains a need for an efficient method for fabricating precisely controlled complex micro/nanostructures.

In this work, we report a facial approach to synthesise AgCl microcrystals with different morphologies including octahedron, trapezohedron (TPH), 12-pod and hexapods with mace pods, as illustrated in Fig. 1. In a typical synthesis, 20 mL ethylene glycol (EG) was sealed in a 50 mL flask, and 200 μL of 1.0 M $AgNO_3$ and 0.8 mL PDDA were added to the flask. After stirring at room temperature for 1 minute, the flask was placed in a 190 °C oil bath. It is worth noting that a specific ionic liquid poly(diallyldimethylammonium chloride) (PDDA) acted as both a Cl^- ion precursor and a morphology-controlled stabilizer. After the reaction was carried out for 30 minutes, the solution became colourless and transparent. Then, the flask was cooled to room temperature. Then after centrifugation, the supernatant was removed to obtain the product. Characterization was carried out after washing twice with water and ethanol, respectively. In addition, AgCl crystals with different morphologies, which include octahedron, trapezohedron (TPH), 12-pod and hexapods with mace pods, were prepared by adding NaCl to adjust the concentration of Cl^- ions (see the details in the Experimental section). Furthermore, by systematically exploring the influence of reaction conditions, we explored the growth mechanism of 3D AgCl crystals with different morphologies. We found that the 3D AgCl microstructures all evolved from the initial octahedral structure, and the intermediate state of the structure evolution was captured by precisely regulating the reaction conditions.

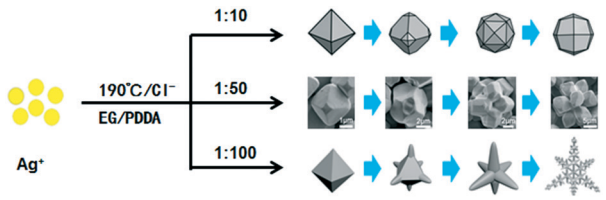

Fig. 1 Illustration of the formation process of TPH, 12-pod and hexapods with mace pods of AgCl crystals.

Experimental section

Chemicals

All reagents and solvents were purchased from commercial sources and used as received without further purification. Chemicals used in this study included silver nitrate ($AgNO_3$, A.R. 99.8%, Sinopharm Group Reagent Co., Ltd., Shanghai, China), hydrochloric acid (HCl, AR), sodium chloride (NaCl, AR, 36.0–38.0%) nitric acid (HNO_3, AR, 65.0–68.0%), ethylene glycol (EG), and poly(diallyldimethylammonium chloride) (PDDA, MW = 200 000–350 000 D, 20 wt% in H_2O, ≥99%), which were purchased from Aladdin. The solutions were prepared from super pure water (18 MΩ cm) purified using a Milli-Q Lab system (Nihon Millipore Ltd.).

Synthesis of AgCl microstructures with different morphologies

The AgCl microstructures with different morphologies were selectively synthesized *via* Cl^--induced precipitation from a silver nitrate precursor. Briefly, different amounts of NaCl powder were added to a 50 mL flask containing 20 mL of EG solution with vigorous stirring of the magnets. Stirring was continued at room temperature until NaCl was completely dissolved and then 0.8 mL of PDDA solution was added. Subsequently, 200 μL of 1.0 M $AgNO_3$ solution was added and subjected to vigorous stirring for 5 min. Upon addition of $AgNO_3$, the transparent solution immediately turned milky white, indicating the formation of solid AgCl. Then, the mixture was placed in an oil bath at 190 °C under vigorous stirring for 30 min. After heating, the milky white solution became colourless and transparent. After 30 minutes of reaction, the heating was switched off and cooled to room temperature. During the cooling process, the solution gradually became cloudy and opaque, indicating that AgCl crystals were precipitated. All glassware used in the experiment were washed with freshly prepared aqua regia ($HCl:HNO_3$ = 3:1) for 30 minutes and then thoroughly rinsed twice with ultrapure water and ethanol, respectively. When the reaction was expected to be completed, the supernatant was removed by centrifugation at 12 000 rpm for 15 minutes, the product was ultrasonically dispersed in ethanol and water, and then washed twice. Prepared AgCl particles were then dispersed in an ethanol solution for further use.

Characterization

The morphologies and structures of the prepared AgCl crystals were characterized using a scanning electron microscope (SEM, 3.0 kV, SU70, Hitachi, Japan) and an X-ray diffractometer (XRD, Cu Kα1 radiation, Rigaku/Ultima IV, Japan). The diffraction pattern was recorded in the range of 20–80 degrees. In addition, energy-dispersive X-ray

spectroscopy (EDS) mapping was also used to characterize the prepared crystals.

Results and discussion

In a typical synthesis, 20 mL of EG was sealed in a 50 mL flask, and then different amounts of NaCl powder were added to the EG solution and stirred at room temperature until the NaCl was completely dissolved. Subsequently, 200 μL of 1.0 M $AgNO_3$ and 0.8 mL PDDA were added to the flask. As soon as the $AgNO_3$ solution was added, it became opaque immediately, which indicated that AgCl precipitation occurred. We centrifuged the AgCl precipitate at this time, and the SEM picture is presented in Fig. S5.† After stirring at room temperature for 1 minute, the flask was placed in a 190 °C oil bath for reaction. The solution became clear and transparent after 30 minutes of reaction at 190 °C. The solution was subsequently cooled to room temperature and a milky white precipitate appeared. The AgCl precipitate was obtained by centrifugation at 12 000 rpm, and the obtained precipitate was washed twice with water and ethanol, respectively. In this process, we think that the AgCl crystals are dissolved at high temperatures, and hence, the mixed solution becomes colourless and transparent. In the reaction system, the concentration of Cl^- is much higher than the concentration of Ag^+. We conclude that in a high Cl^- environment, the initially formed AgCl (K_{sp} = 1.77 × 10^{-10}) precipitate was transformed into $AgCl_2^-$ (K_f = 2.5 × 10^{-5}). When the reaction stopped, $AgCl_2^-$ gradually crystallized and AgCl crystals were precipitated as the solution cooled to room temperature.[45,46]

Fig. 2A presents the SEM images of the as-prepared AgCl crystals with TPH morphology, which was synthesised at Ag^+/Cl^- = 1/10. In addition, we found that the AgCl size of the TPH morphology will increase as the amount of NaCl increases, as shown in Fig. 2B–D. We can see that the yield of AgCl crystals with TPH morphology is close to 100%. Previous studies on high-index facet noble metal crystals have shown that the TPH structure is composed of 24 high-index {*hkk*} (*h* > *k*) facets.[41,42] Since AgCl crystals will be reduced to Ag due to long-term exposure to high-current density electron beams, the crystal plane index of TPH structure AgCl crystals cannot be determined directly by TEM characterization and the corresponding selected area electron diffraction (SAED).[43] Therefore, we used a method of determining the projection angle along a specific crystal axis to determine its crystal plane. The corresponding Miller index can be determined using the projection angle of the TPH AgCl crystals in the <100> direction (Fig. 2E). As shown in Fig. 2E, the average measured values of α and β were 143.3° and 127.0°, respectively. This result is in good agreement with the theoretical value corresponding to the {311} crystal plane. Therefore, the prepared TPH-form AgCl crystal is composed of 24 high-index {311} facets. The SEM images of TPH AgCl crystals at different angles (Fig. 2F–I) further demonstrate the TPH geometry of AgCl crystals.

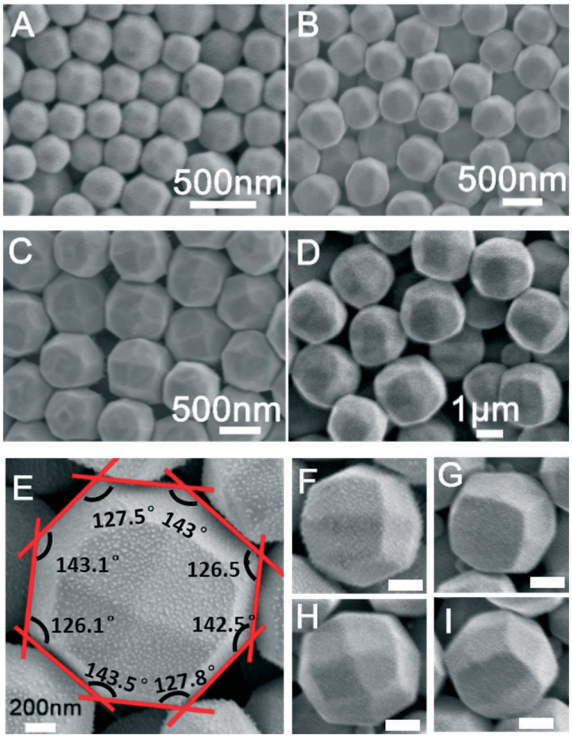

Fig. 2 SEM images of AgCl crystals with different TPH morphologies. (A) 200 nm, (B) 250 nm, (C) 500 nm, and (D) 600 nm. (E) SEM image of a single TPH AgCl crystal viewed from the <100> direction. (F–I) Individual TPH AgCl crystals in different orientations. Scale bar: 500 nm.

When the molar ratio of Ag^+/Cl^- was reduced to 1/50, the shape of AgCl crystals transformed from TPH to 12-pod, which can be seen in the SEM images of Fig. 3. To the best of our knowledge, this is the first report of the 12-pod AgCl crystals. As shown in Fig. 3A, we can see the detailed

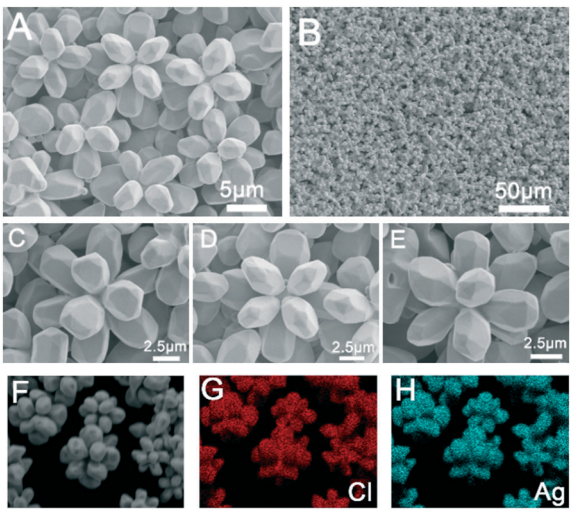

Fig. 3 SEM images of flower-like AgCl crystals: (A) high magnification and (B) low magnification. (C–E) Individual flower-like AgCl crystals in different orientations. (F–H) EDS elemental mapping of hollow Au crystals indicating the Cl and Ag elemental distribution.

structure of the 12-pod AgCl crystals. The sizes of the 12-pod AgCl crystals range from 10 to 15 μm, with an average pod length of around 5 μm. From the low-magnification SEM image (Fig. 3B), we can see that 12-pod AgCl has good uniformity. Fig. 3C–E shows the SEM images of different orientations of a single 12-pod AgCl crystal. By analysing its structure, we can determine that the AgCl crystal is composed of 12 pods. In addition, we can see that each branch is composed of many different flat faces, and subsequent studies on the growth mechanism of AgCl crystals will further confirm its structural composition and surface structure. Furthermore, the 12-pod AgCl microcrystals were further identified by energy-dispersive X-ray spectroscopy (EDS). EDS mapping (Fig. 3G and H) clearly shows that Ag and Cl are uniformly distributed throughout the AgCl crystals.

As shown in Fig. 4, when the molar ratio of Ag^+/Cl^- was further reduced to 1/100, the morphology of the prepared AgCl crystals will change to hexapods with mace pods. Fig. 4A and B show the high-magnification and low-magnification SEM images of AgCl crystals with hexapod with mace pod morphologies, respectively. This phenomenon is in agreement with our previous reports.[44] Fig. 4C and D show the SEM micrographs of the hexapods with mace pods of the AgCl crystal structure viewed from different directions. Previous research reports indicate that AgCl crystals with hexapods with mace pods are grown from octahedrons to form a six-pod structure. The six-pod structure further grows on each pod to form a structure with hexapods with mace pods. Different from previous reports, we found that with the further increase in Cl^- concentration, the branches of the prepared AgCl crystal with hexapods with mace pods will grow further, as shown in the red circle in Fig. 4C. We can see that small rod-like structures will continue to grow on the branches of the AgCl crystal with hexapods with mace pods.

We further explored the factors including temperature, ligand, precursor concentration and metal ions affecting the formation of AgCl crystals with different morphologies. First, we study the effect of temperature on the growth of AgCl crystals. While keeping other conditions constant, we tested the effects of a series of reaction temperatures on the growth of AgCl crystals. We found that when the reaction temperature is higher than 180 °C, we will get AgCl crystals with a uniform morphology and size. However, when the reaction temperature is lower than 180 °C, AgCl crystals with irregular morphology will be obtained. Fig. S1 and S2† show the SEM micrographs of AgCl crystals prepared at reaction temperatures of 170 °C and 190 °C, respectively. Furthermore, we explored the effect of PDDA on AgCl crystal growth. As we mentioned above, PDDA is used not only as a ligand for regulating morphology, but also as a source of Cl^-. Keeping the other conditions unchanged, we used NaCl instead of PDDA to provide Cl^-, and we got completely different results. As shown in Fig. 5, in the absence of PDDA, different amounts of NaCl were added to provide Cl–, and a series of AgCl crystals with different morphologies were prepared. As shown in Fig. 5A, when $Ag^+/Cl^- = 1/10$, we obtain cubic AgCl crystals. When the molar ratio of $Ag^+/Cl^- = 1/20$, the cubic AgCl crystals preferentially grow along the edges and corners to form concave cubes, as shown in Fig. 5B. Upon continuous increase in the amount of NaCl, AgCl cubes will grow further along the edges and corners to form the octopod structure, as shown in Fig. 5D. This phenomenon is in agreement with previous reports that cubic AgCl crystals preferentially grow along the <111> and <110> directions when the Cl^- concentration is increased.[38–40] Furthermore, we explored the role of Cl^- in the growth of AgCl crystals. Keeping other reaction conditions unchanged (200 μL of 1.0 M $AgNO_3$ and 0.8 mL PDDA), we adjusted the concentration of Cl^- by changing the amount of NaCl added. As shown in Fig. S3–S8,† when the amount of NaCl is 15 mg, 30 mg, 90 mg, 120 mg, 150 mg, and 165 mg, the TPH AgCl we obtained are 200 nm, 250 nm, 500 nm, 600 nm, 1.0 μm and 2.0 μm, respectively. We can find that when the Cl^- concentration is relatively low, AgCl crystals prepared have a TPH morphology, and the AgCl crystal size of TPH will

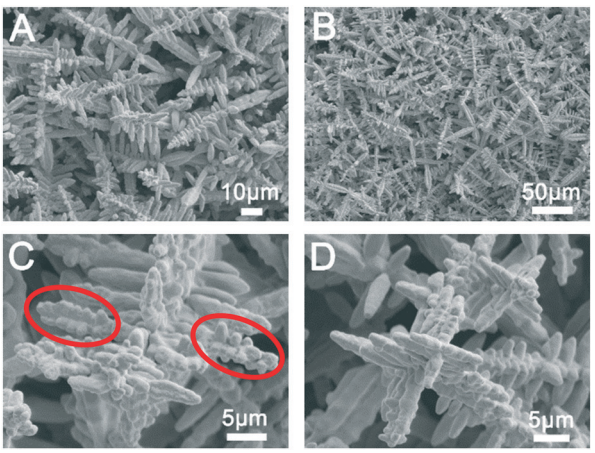

Fig. 4 SEM images of hexapod with mace pod AgCl crystals: (A) high magnification and (B) low magnification. (C and D) Individual hexapod with mace pod AgCl crystals in different orientations.

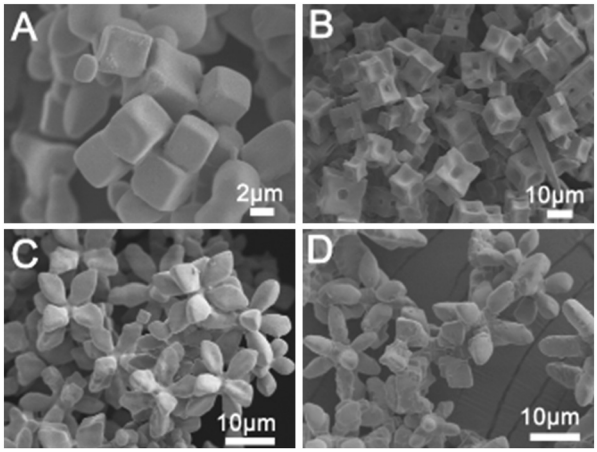

Fig. 5 SEM images of AgCl crystals synthesized without PDDA. (A) $Ag^+/Cl^- = 1/10$, (B) $Ag^+/Cl^- = 1/20$, (C) $Ag^+/Cl^- = 1/30$, and (D) $Ag^+/Cl^- = 1/50$.

gradually increase with the increase in the Cl^- concentration. When the amount of NaCl was increased to 200 mg, we obtained 12-pod AgCl crystals, as shown in Fig. 3. As the amount of NaCl continued to increase to 350 mg, rod-shaped AgCl crystals gradually appeared in 12-pod AgCl crystals, as shown in Fig. S9.† Furthermore, when we add 400 mg of NaCl to further increase the concentration of Cl^- in the solution, AgCl crystals with hexapods with mace pods will be prepared, and until NaCl is increased to 700 mg, the AgCl crystals will have an irregular and disordered morphology (Fig. S10†). The 3D AgCl microcrystals prepared in the experiment were also characterized by X-ray diffraction (XRD), and the product map (Fig. 6) was compared with the map of JCPDS NO. 85-1355 in the database. The XRD lines shown in Fig. 6a–d correspond to octahedron, TPH, 12-pod and hexapod with mace pod AgCl microcrystals, respectively. We can see that there are no additional impurity peaks in the XRD pattern of AgCl microcrystals, and these peaks are symmetric, indicating that the crystal structure of AgCl crystal is of high quality. According to previous reports, metal ions will affect the morphology of semiconductor nanoparticles.[48] Therefore, we used KCl, $MgCl_2$ and $CaCl_2$ instead of NaCl as the source of Cl– ions without changing other conditions, and explored the effects of different metal ions on the growth of AgCl crystals. Fig. S12–S14† show respectively the SEM images of AgCl crystals prepared using KCl, $MgCl_2$ and $CaCl_2$ as the source of Cl-ions. We can see that the morphologies of AgCl crystals prepared under different metal ion conditions are consistent with those when NaCl is used. It shows that different metal ions have no obvious influence on the morphology of AgCl crystals in this experiment.

In order to further explore the formation mechanism of AgCl crystals with different morphologies, we reduced the $AgNO_3$ concentration and changed the Ag^+ concentration to explore its growth pattern. We reduced the $AgNO_3$ concentration to 0.1 M and fixed PDDA to 0.8 mL. By changing the volume of $AgNO_3$ used, we obtained the morphological evolution process of AgCl crystals with different morphologies. As shown in Fig. 7A and 8A, when we add 600 μL of 0.1 M $AgNO_3$ solution, we will get octahedral

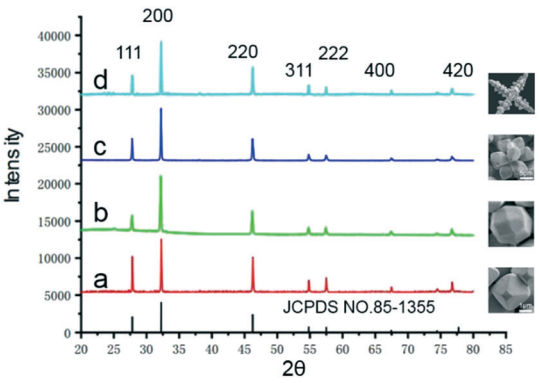

Fig. 6 XRD patterns of the as-prepared AgCl crystals. (a) Octahedron; (b) TPH; (c) flower-like; (d) hexapods with mace pods.

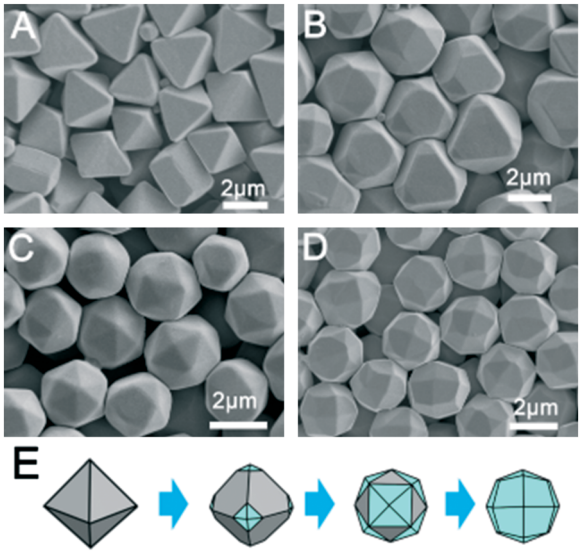

Fig. 7 (A–D) SEM images of AgCl microcrystals at different amounts of 0.1 M $AgNO_3$ solution: (A) 600 μL; (B) 650 μL; (C) 700 μL; and (D) 750 μL. (E) Illustration of shape transformation of AgCl crystals from octahedra to TPH.

AgCl crystals with a size of about 2.0 μm. From Fig. 7 we can see that as the amount of silver nitrate increases, the AgCl crystal gradually changes from octahedron to TPH. Keeping the other conditions constant, adding 600 μL of 0.1 M $AgNO_3$ solution will result in AgCl crystals with a size of 2.0 μm (Fig. 7A). When the amount of $AgNO_3$ added is increased to 650 μL, the size of the octahedron AgCl crystals decreases and the shape transformation starts at the vertices (Fig. 7B). This process is similar to our previous report.[15] At this time, the {111} facets of the octahedron are converted into regular

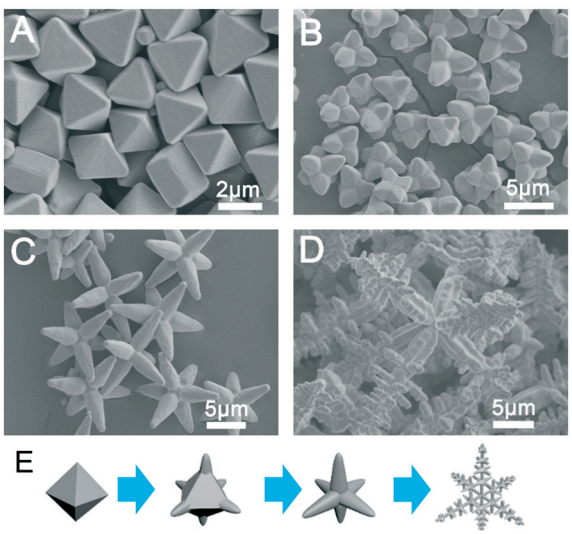

Fig. 8 SEM images of AgCl microcrystals at different amounts of 0.1 M $AgNO_3$ solution: (A) 600 μL; (B) 550 μL; (C) 500 μL; and (D) 400 μL. (E) Illustration of shape transformation of AgCl crystals from octahedra to hexapods with mace pods.

hexagons, and each vertex of the original octahedron is capped by a square-based pyramid. With further truncation and growth, the truncated octahedron will transform into a regular polyhedron composed of 8 low-index {111} facets and 24 high-index {311} facets (Fig. 7C). As the amount of $AgNO_3$ continues to increase, the {111} facets of the octahedron will continue to decrease, while the {311} facets continue to increase. When the amount of $AgNO_3$ added up to 750 μL, the {111} facets completely disappeared, and the AgCl crystal was converted from octahedron to TPH (Fig. 7D). As can be seen from Fig. 7D, the crystal size of the TPH morphology of AgCl is about 2.0 μm. Fig. 7E shows the corresponding shape transformation model of AgCl crystals. Conversely, when we reduce the amount of $AgNO_3$, the AgCl crystal will change from octahedron to hexapods with mace pods, which is consistent with our previous reports.[44] AgCl octahedrons will preferentially grow along the <100> direction (Fig. 8B). With the decrease of $AgNO_3$, the six vertices of the AgCl octahedron are pulled out to form a hexapod structure. The hexapod AgCl will continue to grow along the <100> direction, eventually forming hexapods with mace pods. The formation of 12-pod AgCl crystals is very sensitive to Ag^+ and Cl^- concentration. When we fixed PDDA = 0.8 mL ($n(Cl^-)$ = 1 mmol) and slightly changed the amount of $AgNO_3$, we obtained the morphological transformation, as shown in Fig. 9A–C. When we added 200 μL of 1 M $AgNO_3$ solution and slightly changed the amount of NaCl added, we further obtained the morphological transformation, as shown in Fig. 9D–F. As shown in Fig. 9A, when 600 μL $AgNO_3$ is added, uniform octahedral AgCl crystals with a size of about 2.0 μm is prepared. When the amount of $AgNO_3$ is increased to 610 μL, as the octahedral AgCl crystal grows, its apex will appear "dented". As shown in Fig. 9B, each vertex of the octahedron appears as a cube-shaped depression. As the amount of $AgNO_3$ continues to increase to 620 μL, the eight faces of the octahedral AgCl crystal also begin to appear "depressed." As shown in Fig. 9C, each vertex of the octahedron exhibits a depression in the shape of a cube, and at the same time, a depression in the shape of a pyramid appears on each face. With the further depression of each vertex and face of the octahedron, the shape shown in Fig. 9D will appear. At this time, the original octahedron will be split into 12 polyhedra and connected together. On the basis of Fig. 9D, we further reduce the amount of NaCl, and the AgCl crystal will be transformed into a shape with 12 octahedra connected together (Fig. 9E). Continue to reduce the amount of NaCl, the 12 octahedrons began to transform to TPH morphology (Fig. 9F), and started at the vertices. Fig. 9G is the SEM image of a single-particle 12-pod AgCl crystal formation process. In Fig. 9G2–4, we can clearly see the depression shape of the octahedron AgCl on the vertices and faces. In Fig. 9G5, we can clearly see the morphology of AgCl crystals with 12 octahedral connection. Comparing Fig. 9G5 and G6, we can clearly see that the 12 octahedrons connected together begin to transform into the TPH form, starting from the vertical of each octahedron.

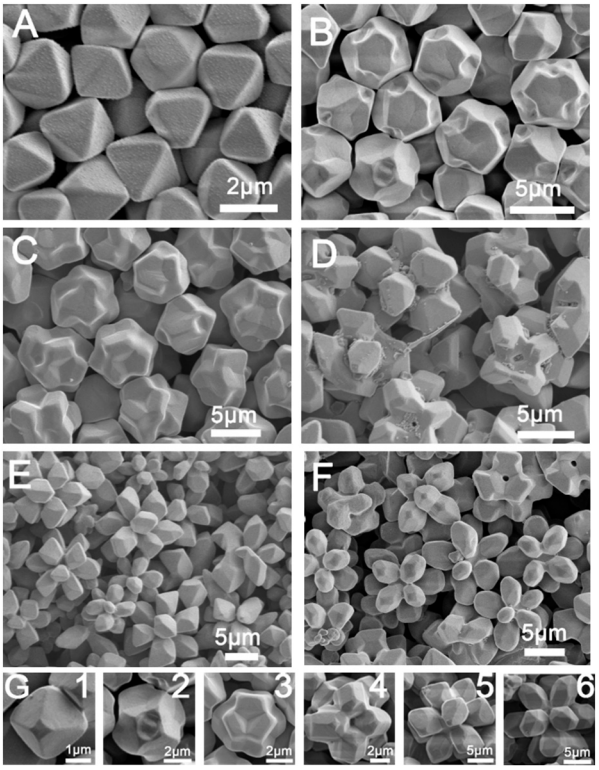

Fig. 9 SEM images of AgCl microcrystals at different amounts of 0.1 M $AgNO_3$ solution: (A) 600 μL; (B) 610 μL; and (C) 620 μL. SEM images of AgCl microcrystals at different amounts of NaCl: (D) 350 mg; (E) 310 mg; and (F) 300 mg. (G1–G6) Single-particle flower-like AgCl crystal formation process.

Based on the above-mentioned experimental results, we deduced a possible mechanism for the growth of AgCl crystals with different morphologies. At room temperature, as soon as Ag^+ encounters Cl^- (whether from PDDA or NaCl), AgCl precipitates immediately (Fig. S11†). Then, in a high-Cl^- concentration environment and at high temperatures, AgCl will gradually dissolve and change to $AgCl_2^-$. When there is no PDDA, as the reaction ends, the temperature of the solution decreases. $AgCl_2^-$ will crystallize into AgCl cubes with a lower surface energy. As Cl^- increases, cubic AgCl will preferentially grow along the <111> and <100> directions, eventually forming an eight-pod AgCl crystals (Fig. 5D). When PDDA is added as a morphology modifier, the AgCl crystals will preferentially form an octahedral structure. This is consistent with previous reports that PDDA is adsorbed on the {111} crystal plane during the nucleation of face-centred cubic (FCC) crystals.[47] With the increase in the Cl^- concentration, the octahedron AgCl crystal will grow preferentially along the <110> direction. The octahedron is elongated along the apex direction, and finally, a six-pod AgCl crystal is formed. In contrast, with the decrease in the Cl^- concentration, the growth of the apex and surface of the octahedral AgCl is inhibited and the 12-pod structure is formed. When the Cl^- is further reduced, octahedral AgCl will transform to the TPH morphology, which is enclosed by 24 high-index {311} facets.

Conclusions

In summary, we have successfully prepared octahedron, TPH, 12-pod and six-rod AgCl crystals by a one-pot PDDA-mediated polyol synthesis method. In addition, by fine-tuning the experimental conditions, we achieved the shape transformation of AgCl octahedron to TPH at a relatively lower Cl^- ion concentration, the transition of octahedron to 12-pod morphology at moderate Cl^- ion concentration and the morphology evolution of octahedron to hexapods with mace pods, under high Cl^- ion concentration. Furthermore, we explored the effects of various factors on the growth of AgCl crystals. Meanwhile, TPH-morphology AgCl crystals with a controllable size of 200 nm–2 μm were synthesised by simply changing the amount of NaCl. We believe that this work not only provides a simple method for preparing AgCl crystals with different regular morphologies, but also provides new insights into crystal growth habits.

Conflicts of interest

There are no conflicts to declare.

Acknowledgements

Financial supported by the National Key Research and Development Program of China (No. 2018YFC0807404 and No. 2016YFC0800906) and the Technology Research Program of the Ministry of Public Security (No. 2016JSYJA32) are gratefully acknowledged.

Notes and references

1 D. Wang and Y. Li, *Adv. Mater.*, 2011, **23**, 1044–1060.
2 Z. Y. Zhou, N. Tian, J. T. Li, I. Broadwell and S. G. Sun, *Chem. Soc. Rev.*, 2011, **40**, 4167.
3 H. Zhang, M. Jin and Y. Xia, *Chem. Soc. Rev.*, 2012, **41**, 8035–8049.
4 Y. Z. Qin, Y. X. Lu, W. F. Pan, D. D. Yu and J. G. Zhou, *RSC Adv.*, 2019, **9**, 10314–10319.
5 Z. Niu, N. Becknell, Y. Yu, D. Kim, C. Chen, N. Kornienko, G. A. Somorjai and P. Yang, *Nat. Mater.*, 2016, **15**, 1188–1194.
6 J. H. Choi, H. Wang, S. J. Oh, T. Paik, P. Sung, J. Sung, X. Ye, T. Zhao, B. T. Diroll, C. B. Murray and C. R. Kagan, *Science*, 2016, **352**, 205–208.
7 A. Leonardi and M. Engel, *ACS Nano*, 2018, **12**, 9186–9195.
8 N. S. R. Satyavolu, L. H. Tan and Y. Lu, *J. Am. Chem. Soc.*, 2016, **138**, 16542–16548.
9 M. H. Huang and P. H. Lin, *Adv. Funct. Mater.*, 2012, **22**, 14.
10 C. Kinnear, T. L. Moore, L. R. Lorenzo, B. R. Rutishauser and A. P. Fink, *Chem. Rev.*, 2017, **117**, 11476–11521.
11 G. A. Somorjai, *Science*, 1985, **227**, 902.
12 Z. Quan, Y. Wang and J. Fang, *Acc. Chem. Res.*, 2013, **46**, 191–202.
13 J. W. Hong, S. U. Lee, Y. W. Lee and S. W. Han, *J. Am. Chem. Soc.*, 2012, **134**, 4565–4568.
14 W. Niu, W. Zhang, S. Firdoz and X. Lu, *J. Am. Chem. Soc.*, 2014, **136**, 3010.
15 Y. Z. Qin, W. F. Pan, D. D. Yu, Y. X. Lu, W. H. Wu and J. G. Zhou, *Chem. Commun.*, 2018, **54**, 3411–3414.
16 D. Huo, H. M. Ding, S. Zhou, J. Li, J. Tao, Y. Q. Ma and Y. N. Xia, *Nanoscale*, 2018, **10**, 11034.
17 W. Wang, C. X. Wu, J. Zhu, Y. C. Han, Y. Fan and Y. Wang, *CrystEngComm*, 2018, **20**, 7631–7636.
18 D. R. Lide, *CRC Handbook of Chemistry and Physics*, CRC, 88th edn, 2008.
19 P. Wang, B. Huang, X. Qin, X. Zhang, Y. Dai, J. Wei and M. H. Whangbo, *Angew. Chem., Int. Ed.*, 2008, **47**, 7931–7933.
20 H. B. Zhang, Y. G. Lu, H. Liu and J. Z. Fang, *Nanoscale*, 2015, **7**, 11591–11601.
21 R. Dong, B. Tian, C. Zeng, T. Li, T. Wang and J. Zhang, *J. Phys. Chem. C*, 2012, **117**, 213–220.
22 L. Cheng, C. Ma, G. Yang, H. You and J. Fang, *J. Mater. Chem. A*, 2014, **2**, 4534–4542.
23 Q. Zhang, J. Ge, T. Pham, J. Goebl, Y. Hu, Z. Lu and Y. Yin, *Angew. Chem., Int. Ed.*, 2009, **48**, 3516–3519.
24 P. Wang, B. B. Huang, Z. Z. Lou, X. Y. Zhang, X. Y. Qin, Y. Dai, Z. K. Zheng and X. N. Wang, *Chem. – Eur. J.*, 2010, **16**, 538–544.
25 M. Zhu, P. Chen and M. Liu, *Langmuir*, 2013, **29**, 9259–9268.
26 C. An, S. Peng and Y. Sun, *Adv. Mater.*, 2010, **22**, 2570–2574.
27 R. Dong, B. Tian, C. Zeng, T. Li, T. Wang and J. Zhang, *J. Phys. Chem. C*, 2012, **117**, 213–220.
28 Z. Lou, B. Huang, Z. Wang, X. Qin, X. Zhang, Y. Liu, R. Zhang, Y. Dai and M. H. Whangbo, *Dalton Trans.*, 2013, **42**, 15219–15225.
29 Y. H. Ao, J. Q. Bao, P. F. Wang and C. Wang, *J. Alloys Compd.*, 2017, **698**, 410–419.
30 X. Y. Guo, D. Deng and Q. H. Tian, *Powder Technol.*, 2017, **308**, 206–213.
31 Y. T. An, W. R. Cao, Y. Y. Zhou, L. F. Chen and Z. W. Qi, *Appl. Organomet. Chem.*, 2017, **31**, 3777–3787.
32 Y. Tang, Z. Jiang, G. Xing, A. Li, P. D. Kanhere, Y. Zhang, T. C. Sum, S. Li, X. Chen, Z. Dong and Z. Chen, *Adv. Funct. Mater.*, 2013, **23**, 2932–2940.
33 S. H. Han, H. M. Liu, C. C. Sun, P. J. Jin and Y. Chen, *J. Mater. Sci.*, 2018, **53**, 12030–12039.
34 Y. P. Bi and J. H. Ye, *Chem. Commun.*, 2009, 6551–6553.
35 Y. P. Bi and J. H. Ye, *Chem. Commun.*, 2010, **46**, 1532–1534.
36 H. Y. Hu, Z. B. Jiao, G. X. Lu, J. H. Ye and Y. P. Bi, *RSC Adv.*, 2014, **4**, 31795–31798.
37 J. Liao, K. Zhang, L. J. Wang, W. Z. Wang, Y. G. Wang, J. G. Xiao and L. Yu, *Mater. Lett.*, 2012, **83**, 136–139.
38 Z. Lou, B. Huang, X. Qin, X. Zhang, H. Cheng, Y. Liu, S. Wang, J. Wang and Y. Dai, *Chem. Commun.*, 2012, **48**, 3488–3490.
39 Z. Lou, B. Huang, X. Ma, X. Zhang, X. Qin, Z. Wang, Y. Dai and Y. Liu, *Chem. – Eur. J.*, 2012, **18**, 16090–16096.
40 H. Gatemala, C. Thammacharoen and S. Ekgasit, *CrystEngComm*, 2014, **16**, 6688–6696.
41 Z. Quan, Y. Wang and J. Fang, *Acc. Chem. Res.*, 2013, **46**, 191–202.

42 Y. Li, Y. Jiang, M. Chen, H. Liao, R. Huang, Z. Zhou, N. Tian, S. Chen and S. Sun, *Chem. Commun.*, 2012, **48**, 9531–9533.
43 C. An, S. Peng and Y. Sun, *Adv. Mater.*, 2010, **22**, 2570–2574.
44 Y. X. Lu, Y. Z. Qin, D. D. Yu and J. G. Zhou, *Crystals*, 2019, **9**, 401.
45 H. Gatemala, S. Ekgasit and P. Pienpinijtham, *CrystEngComm*, 2017, **19**, 3808–3816.
46 S. C. Abeyweera, K. D. Rasamani and Y. Sun, *Acc. Chem. Res.*, 2017, **50**, 1754–1761.
47 K. L. Shuford, M. Chen, E. J. Lee and S. O. Cho, *ACS Nano*, 2008, **2**, 1760–1769.
48 W. Li, R. Zamani, M. Ibáñez, D. Cadavid, A. Shavel, J. R. Morante, J. Arbiol and A. Cabot, *J. Am. Chem. Soc.*, 2013, **135**, 4664–4667.